Ab initio study of the alternating current impedance of a molecular junction

Roi Baer[a)]
Institute of Chemistry and the Lise Meitner Minerva-Center for Quantum Chemistry, the Hebrew University of Jerusalem, Jerusalem 91904 Israel

Tamar Seideman
Department of Chemistry, Northwestern University, Evanston, Illinois 60208-3113

Shahal Ilani
Department of Physics, The Weizmann Institute of Science, Rehovot, 76100 Israel

Daniel Neuhauser
Department of Chemistry and Biochemistry, University of California in Los Angeles, Los Angeles, California 90095-1569

(Received 18 August 2003; accepted 19 November 2003)

The small-bias conductance of the C_6 molecule, stretched between two metallic leads, is studied using time-dependent density functional theory within the adiabatic local density approximation. The leads are modeled by jellium slabs, the electronic density and the current density are described on a grid, whereas the core electrons and the highly oscillating valence orbitals are approximated using standard norm-conserving pseudopotentials. The jellium leads are supplemented by a complex absorbing potential that serves to absorb charge reaching the edge of the electrodes and hence mimic irreversible flow into the macroscopic metal. The system is rapidly exposed to a ramp potential directed along the C_6 axis, which gives rise to the onset of charge and current oscillations. As time progresses, a fast redistribution of the molecular charge is observed, which translates into a direct current response. Accompanying the dc signal, alternating current fluctuations of charge and currents within the molecule and the metallic leads are observed. These form the complex impedance of the molecule and are especially strong at the plasmon frequency of the leads and the lowest excitation peak of C_6. We study the molecular conductance in two limits: the strong coupling limit, where the edge atoms of the chain are submerged in the jellium and the weak coupling case, where the carbon atoms and the leads do not overlap spatially. [DOI: 10.1063/1.1640611]

I. INTRODUCTION

Recently a surge of developments in synthetic and analytic molecular scale methods[1–13] has made possible the realization of the concept of molecular junction electronics.[14,15] This is an emerging field of research, where molecules connected to electrodes conduct electricity under voltage bias. The next step is connecting several molecular junctions to each other. What kind of electronic systems do we expect to result? In classical electronics circuits, predicting the behavior of a system composed of several components is facilitated by the concept of the complex impedance $Z(\omega)$. This is the alternating current (ac) analog of the current–voltage relationship, relating the sinusoidal current passing through a junction, $I(\omega)$, to the sinusoidal voltage bias of the electrodes

$$V(\omega)=Z(\omega)I(\omega). \tag{1.1}$$

Once each component is characterized by an impedance Z_i, the impedance of two components connected serially is $Z_{12,s}=Z_1+Z_2$, whereas that of two components connected in parallel is[16] $Z_{12,p}=(Z_1^{-1}+Z_2^{-1})^{-1}$. The concept should also be useful in molecular electronics, where high-frequency fields can be generated either by the components themselves or by external optical perturbations.

ac conductance in molecular systems has not been studied extensively. In model systems, such as a double barrier or a wire with interacting electrons (Lüttinger liquid), interesting studies, including exact solutions, have been reported.[17–19] It was found useful to compare to standard resistor–capacitor–inductor analogs. A related *but different* issue is the effect an ac field has on the dc conductance.[20] Several interesting articles were published recently by Tikhonov, Coalson, and Dahnovsky[21,22] studying this effect using a combination of Floquet and Green's function formalism that takes into account the time-dependent periodic effects of the laser field. They applied their method, within a tight binding model, to a xylyl–dithiol molecule connected to two electrodes. They found that experimentally accessible laser pulses can significantly enhance the tunneling current through the device. Another related recent work by Lehman *et al.*[23,24] suggests a coherent ratchet mechanism by which oscillating laser fields can produce rectified current in molecular wires.

[a)]Electronic mail: roi.baer@huji.ac.il

The study of dc molecular conductance is discussed in much greater detail in recent years. Most of the approaches are based on the Landauer formula,[25–27] where the conductance is expressed in terms of the quantum-mechanical transmittance of electrons at the Fermi energy. Early applications of Landauer's theory used simplified models (tight binding or ''frozen'' Hartree–Fock/density-functional Hamiltonians), with the goal of exploring new phenomena and gaining insight into the general features of molecular conductance.[28–33] The drawback of the frozen SCF approaches is that they do not allow for the response of the electrons to the bias voltage. The importance of such effects has been established by several workers.[34–40] The nonequilibrium Green's function (NEGF) approach provides a means of accounting for these effects (mostly for dc response) within the Landauer formalism.[26,40–44]

This paper presents a method for computing the impedance and conductance of a molecular system in the small-bias, zero-temperature regime. The basic vehicle is time-dependent density functional theory (TDDFT). We invoke a linear response approach for computing the current–density and voltage–density correlation functions, from which the impedance is calculated using Eq. (1.1). The calculation is performed in the time domain, allowing a glimpse of the current and charge oscillations.

This paper expands, implements, and improves on a recently developed method[45] that can, in principle, incorporate the dynamical effects of electron–electron correlation on conduction. The dc conductance is obtained as the $\omega=0$ inverse impedance. The approach therefore provides also an *ab initio* method of calculating the dc conductance in the limit of low temperature and bias voltage.

The method we describe here naturally accounts for the screening effects for which the NEGF methods were developed. It is interesting to compare the results of the present method and a scattering-DFT type of theory.[36,40,43,44] For this reason, one of the systems we study here is identical to a system studied by Lang and Avouris.[44] Despite the differences in methodology, we find that both methods applied to the same system give essentially identical results. The advantage of the present method (in addition to the ease of extracting ac information) is its rigorous justification, since dynamic electronic excitations from the ground state are explicitly taken into account in the TDDFT formalism.

This article first introduces the basic theory in Sec. II, where conductance and impedance are defined and the methods for their computation are discussed. The model electrodes are also discussed in this section. In Sec. III we present the results of several calculations. We take up two different jellium–C_6–jellium systems. The first, called ''C-system'' is a good conductor: the ends of the wire are submerged in the jellium. The second—the ''R-system,'' is a poor conductor: the ends of the wire are a distance of $2.5\,a_0$ from the respective jellium edges. In both systems we first perform a DFT calculation to determine the basic charge distribution. We find that the C_6 bridge becomes negatively charged when connected to the jellium leads. This result was previously reported by Lang and Avouris[44] for the C-system. We find it holds true also for the R-system, which is less strongly coupled. In order to understand the mechanisms of conductance in these systems, we approach conductance via two routes. First, a very approximate theory is used, which highlights the effect of the ground-state Kohn–Sham effective potential. This is done in Sec. III A. This is the ''frozen''-DFT-Landauer conductance. This analysis, while inaccurate, accentuates an important effect: ''geometric'' resistance; electrons cannot easily flow into the molecular channel because of its narrowness: conductance is efficient only in the C-system, where acceleration in the *perpendicular direction* to the charge flow is present, which also dominates the more accurate calculation done using TDDFT. The results of the more rigorous calculation, based on TDDFT, take into account the screening of the external bias and the dynamics response of the electrons is described in Sec. III B. We then describe the ac response and current in Sec. III C. In Sec. III D we present the ac impedance of the junctions.

II. THEORY METHODS AND MODELS

A. Definition of ac/dc impedance

The definition of conductance we adopt is specialized to a time-dependent approach. We envision two planes, P_1 and P_2, placed deep in the bottom and top electrodes, respectively (see Fig. 1). These planes divide space into three zones: the bottom lead, the interaction zone, and the top lead. The system, initially prepared in its ground state, is subjected to a short weak electromagnetic pulse $\delta\mathbf{E}(t)$. During and after the pulse, the electron number density is time dependent

$$n(\mathbf{r},t)=n_{gs}(\mathbf{r})+\delta n(\mathbf{r},t), \tag{2.1}$$

with $\delta n(\mathbf{r},t)$ depending linearly on $\delta\mathbf{E}$ to first order. The total electrostatic potential is thus time dependent

$$v_e(\mathbf{r},t)=v_{\mathrm{nuc}}(\mathbf{r})+e\,\delta\mathbf{E}(t)\cdot\mathbf{r}+v_H(\mathbf{r},t), \tag{2.2}$$

where $v_{\mathrm{nuc}}(\mathbf{r})$ is the nuclear electrostatic potential experienced by the electrons (assumed static), e is the electron charge, and

$$v_H(\mathbf{r},t)=e^2\int\frac{n(\mathbf{r}',t)}{|\mathbf{r}-\mathbf{r}'|}d^3r' \tag{2.3}$$

is the electronic electrostatic potential (more accurately, the Hartree potential). Note that $v_e(\mathbf{r},t)$ has two sources of first-order time-dependent contributions: the direct effect of $\delta\mathbf{E}$ itself and the accompanying response which acts to *partially screen* it by changing the Hartree potential v_H, resulting from $\delta n(\mathbf{r},t)$.

The electrostatic potential, deep inside each lead (far from the surface or the molecular wire) is assumed to be constant in space. This is because the lead is metallic and large. Thus, any pair of points $\mathbf{r}_1$, $\mathbf{r}_2$ located deep in their respective bottom and top leads can be taken to represent the electrostatic potential of the lead. This electrostatic potential difference is in general time dependent

$$\Delta v(t)=v_e(\mathbf{r}_2,t)-v_e(\mathbf{r}_1,t). \tag{2.4}$$

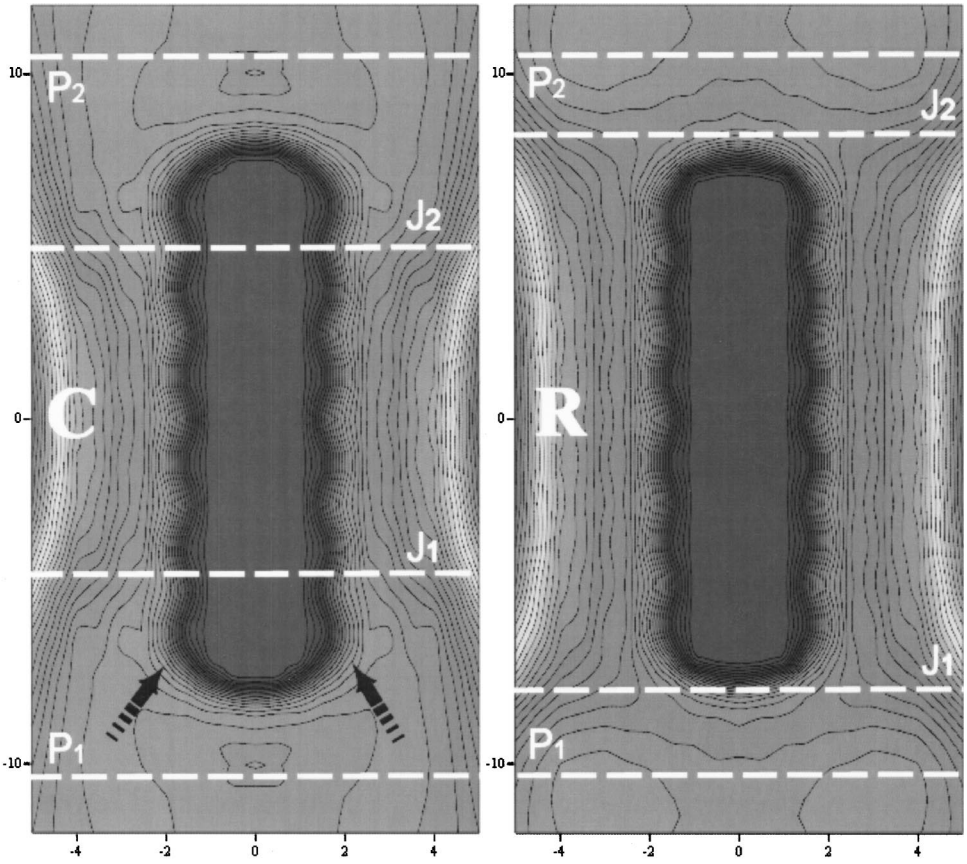

FIG. 1. The Kohn–Sham isopotential contours of the two J–C_6–J systems considered in this paper (the spatial dimensions are in a_0). The C-system has J–J spacing of $D_{JJ}=9.7\,a_0$ and carbon–carbon spacing of $R_{CC}=2.5\,a_0$, while the R-system has $D_{JJ}=16.3a_0$ and $R_{CC}=2.4a_0$. Notice a rainbow coloring of the isopotential contours, with purple the lowest potential and red the highest. The contour spacing potential difference is 1 eV. The arrows in the C-system designate barrierless passage from the jellium to the bridge. The J planes denote the location of the jellium surface.

The electric currents through the two planes, $I_1(t)$ and $I_2(t)$, are not necessarily equal, allowing for time-dependent charge build-up or depletion on the wire

$$\dot{Q}_W(t)=I_2(t)-I_1(t). \tag{2.5}$$

We will consider the average current[18]

$$I(t)=\tfrac{1}{2}(I_1(t)+I_2(t)), \tag{2.6}$$

as the reference current from which we calculate impedance. We note that this choice does not influence the dc conductance,[46] although it will have an effect on the ac impedance. In the dc case this choice improves the convergence (the convergence of the average current in tunneling problems has been considered in detail by Caspary *et al.*[47]).

The ac conductance $G(\tau)$ is defined as the linear kernel relating the current $I(t)$ to the potential difference $\Delta v(t)$

$$I(t)=\int_{-\infty}^{t} G(t-t')\Delta v(t')dt'. \tag{2.7}$$

Note that this is a physically causal relation, expressing the fact that the current is a response to past potential difference. Within the frequency space, the impedance $Z(\omega)$ is the inverse frequency dependent conductance, given by

$$Z^{-1}(\omega)\equiv\tilde{G}(\omega)=\int_0^{\infty} G(t)e^{i\omega t}dt. \tag{2.8}$$

Defining $\Delta\tilde{v}(\omega)=\int_{-\infty}^{\infty}\Delta v(t)e^{i\omega t}dt$ with a similar relation for $\tilde{I}(\omega)$, we arrive at the relation

$$Z^{-1}(\omega)=\tilde{G}(\omega)=\frac{\tilde{I}(\omega)}{\Delta\tilde{v}(\omega)}, \tag{2.9}$$

which also shows the impedance as the inverse of the ac conductance. By definition, the conductance and impedance are *properties of the system*, independent of the small time-dependent perturbation used to calculate them [this drops off when the ratio is taken in Eq. (2.9)].

When the system is exposed to an external electric field, it responds by generating currents and time-dependent charge redistribution. In Eq. (2.9), the numerator contains the current response of the system. But, what about the denominator? A careful consideration shows that it must include, in addition to the external potential difference, the potential response of the system due to the charge reorganization.[18,34,48] These two response contributions, of the numerator and denominator of Eq. (2.9), must be calculated consistently in a single framework.

B. Time-dependent density functional theory

In order to compute the currents and densities following the perturbation, we use the time-dependent density functional theory of Runge–Gross.[49] This theory is exact if an

exact functional is used. In our application we use the adiabatic local density approximation (ALDA). While this approximation can be criticized as being too simplistic for an accurate description of the conduction, it is a good place to start as a first computation. Indeed, it is tempting to use more elaborate functionals, based on the current density.[50,51] At present, however, functionals with the desired features are still untested and appear to have some fundamental problems, such as the impossibility of writing down a consistent action functional.[52] Thus, we defer this issue to a future study.

The equations we solve are thus

$$i\hbar\dot{\varphi}_n(\mathbf{r},t) = -\frac{\hbar^2}{2\mu_e}\nabla^2\varphi_n(\mathbf{r},t) + v_s(\mathbf{r},t)\varphi_n(\mathbf{r},t), \quad (2.10)$$

where $\varphi_n(r,t)$ are the time-dependent Kohn–Sham orbitals $(n=1,...,N)$, the density is given by $n(\mathbf{r},t) = \Sigma_{n=1}^{N_e}|\varphi_n(\mathbf{r},t)|^2$, and the effective potential is a combination of the electrostatic potential [see Eq. (2.2)] and an exchange-correlation term

$$v_s(\mathbf{r},t) = v_e(\mathbf{r},t) + v_{xc}(\mathbf{r},t). \quad (2.11)$$

Within ALDA the latter is given by

$$v_{xc}(\mathbf{r},t) = \varepsilon_{xc}(n(\mathbf{r},t)) + \varepsilon'_{xc}(n(\mathbf{r},t))n(\mathbf{r},t), \quad (2.12)$$

where ε_{xc} is the homogeneous electron gas energy per particle parametrized by Perdew and Wang.[53]

C. Model

We consider two systems, each consisting of an atomic carbon chain, C_6, connected to model gold leads. The first system, which we denote by "C" as it is a good conductor, is identical to the system studied Lang and Avouris[44] (LA). This model consists of 6 carbon atoms stretched between two jellium slabs. The edge atoms are immersed $1.4\,a_0$ inside in the jellium slabs. The second system is similar to the first, but the edge atoms are a bond distance away from the lead surface. This system shows lower conductance and is denoted by "R." The positive spatial density of the jellium slabs is given by

$$n_+(x,y,z) = \frac{n_+}{2}\left(\frac{1}{1+e^{-\alpha(z-z_1)}} + \frac{1}{1+e^{\alpha(z-z_2)}}\right), \quad (2.13)$$

where the z coordinate is defined by the wire axis. The positive jellium density is $n_+ = (4\pi r_s^3/3)^{-1}$, with $r_s = 3a_0$, a value often used to simulate gold. The parameters of both systems are given in Table I.

The electron orbitals and density are described on a grid of spacing $\Delta x, \Delta y, \Delta z$, spanning a box of size L_x, L_y, L_z that contains the system under periodic boundary conditions. The grid parameters are given in Table I. In conjunction with this, fast Fourier methods are used to solve the relevant Poisson equations and to implement the kinetic energy. The replacement of the atomic cores by pseudopotentials allows use of a relatively sparse grid. We use standard Troulier–Martins[54] pseudopotentials, generated by the program of Fuchs and Scheffler.[55]

TABLE I. Various parameters used in the calculations.

Jellium parameters	$\alpha = 3.33\,a_0$, $r_s = 3$ ($n_+ = 0.008\,84\,a_0^{-3}$) System C	System R	Eq. (2.13)
z_1 (a_0)	−18.42	−21.73	
z_2 (a_0)	−4.85	−8.15	
Grid	$(Lx,Ly,Lz) = (10,10,64)\ a_0$, $\Delta x = \Delta y = \Delta z = 0.5\,a_0$		
Negative imaginary potentials	$z_I = 9a_0$, $m=3$, $A = 6.37\times10^{-4}$		Eq. (2.15)
Ramp pulse	$T = 10\ T = 10\ E_h/\hbar$, $E = 10^{-4}\ E_h/q_e a_0$		Eq. (2.21)

D. Energy and particle dissipation

In molecular conductance, the macroscopic leads supply and absorb the charge carriers and are also responsible for dissipating the excess electronic energy. This is an important ingredient in any conductance theory, since for there to be resistance, heat must be dissipated. In the present calculation we absorb the energetic electrons by imposing absorbing boundary conditions, an approach used often in quantum dynamics theories of scattering.[56] The role of the absorbing boundary in molecular conductance calculations has been discussed elsewhere[57] and has been used by several groups in the past (see also the review by Nitzan[58]). Its physical content is that of the imaginary part of the self-energy in nonequilibrium Green's function methods. The absorbance of these particles automatically causes loss of their excess energy and is our source of energy dissipation as well.

Our absorbing potential has the form

$$\hat{\Gamma}_{NIP} = -i\hat{Q}^\dagger\Gamma_{NIP}(\mathbf{r})\hat{Q}, \quad (2.14)$$

where $\hat{Q} = \hat{1} - \Sigma_{n=1}^{N_e}|\varphi_n\rangle\langle\varphi_n|$ is the projector on the Kohn–Sham virtual space, assuring that electrons which are not excited above the Fermi sea are not absorbed. The electrons that can be absorbed "see" a negative imaginary potential localized at the edges of the jellium slabs. We use the optimized form of Riss and Meyer[59]

$$\Gamma_{NIP}(x,y,z) = \begin{cases} 0 & z < z_I \\ -A(z-z_I)^m & z > z_I, \end{cases} \quad (2.15)$$

where the parameters are given in Table I. The absorbing potential of Eq. (2.15) pertains to the bottom jellium slab, Γ_1, and an identical absorber is located at the edge of the top slab, Γ_2.

E. A simplified time-independent approach

Although we focus primarily on developing and applying an approach to conductance calculations within TDDFT, it is instructive to consider also a simpler, complementary approach, within the familiar Landauer formalism. The approach presented in this subsection cannot give a quantitative description of conductance because it does not take into account the shape of the screening bias voltage. It does, how-

ever, include a lot of the physics incorporated into the ground-state potential of the problem, and provides, in addition, a useful reference for the dc conductance.

Using the absorbing potential, we can calculate the conductance from the ''cumulative reaction probability'' which is the Miller–Seideman formula[60]

$$N(E)=4tr\{\hat{G}^{\dagger}(E)\Gamma_1\hat{G}(E)\Gamma_2\}, \tag{2.16}$$

where $\hat{G}(E)=(E-\hat{H}+i\Gamma_1+i\Gamma_2)^{-1}$ is the Green's function of the complex Hamiltonian. This formula is analogous to the nonequilibrium Green's function formula, with Γ_i replaced by the corresponding imaginary parts of the self-energy. This is the analogous quantity to the one-dimensional transmittance $T(E)$. The Landauer formula gives the zero-temperature conductance as related to the cumulative reaction probability at the Fermi energy

$$g=g_0N(E_F), \tag{2.17}$$

where $g_0=2e^2/h$ is the quantum unit of conductance. The computation of the trace in Eq. (2.16) is not an easy task, because of the large grid we use (in the example discussed below, there are over 50 000 grid points). In order to facilitate the calculation, we make use of the fact that Γ are definite in sign, allowing us to write the cumulative reaction probability as a positive definite kernel

$$N(E)=4tr\{S^{\dagger}S\}, \tag{2.18}$$

where $S=\sqrt{\Gamma_L}G(E)\sqrt{\Gamma_R}$. The operation of the Green's function matrix on a vector is implemented using a preconditioned quasiresidual method.[61] Re-expressed in terms of S, the trace can be computed within an efficient Monte Carlo method.[62] Equation (2.18) takes the form

$$N(E)=4\langle\langle\Psi_\Theta|S^{\dagger}S|\Psi_\Theta\rangle\rangle_\Theta, \tag{2.19}$$

where $\Psi_\Theta(r_n)=e^{i\theta_n}$ is a wave function of unit amplitude and random phase θ_n localized at the grid point r_n. Averaging in Eq. (2.19) is done on the uncorrelated random phases based on the fact that $\langle e^{i(\theta_n-\theta_m)}\rangle=\delta_{nm}$.

The typical problem of quantum Monte Carlo methods, namely the sign problem (see for example Ref. 63), is circumvented here because the integrand that is averaged is positive definite. The method is therefore remarkably efficient. In general, the statistical error decreases as $M^{-1/2}$, where M is the number of iterations. Experience shows that the initial error is typically small, and hence averaging over about 150 random functions yields a good estimate, to within 10% of the converged value. The convergence of the Monte Carlo calculation of $N(E)$ is illustrated in Fig. 2.

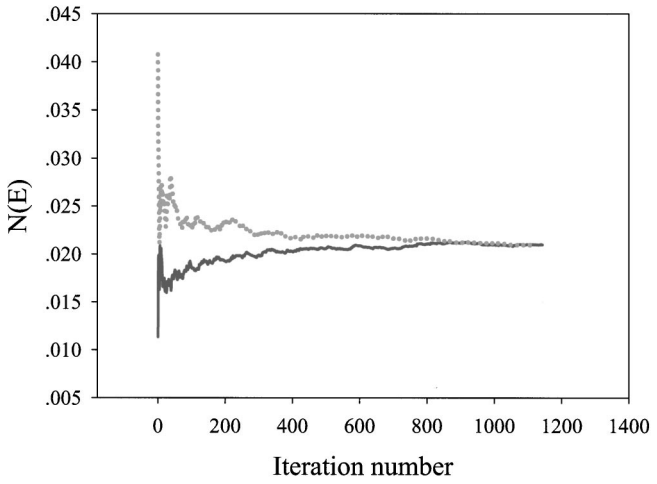

FIG. 2. An example of the Monte Carlo iterations for calculating the conductance of the R-system within the simple Landauer approximation. We show two separate runs, converging to essentially identical statistically significant limits.

III. RESULTS

A. Landauer dc conductance of the C_6 systems

An $x=0$ cut of the Kohn–Sham potential of the two systems is shown in Fig. 1. The deep atomic potential wells that coalesce into an elongated molecular channel connecting the two electrodes are clearly observed. A cut at $x=y=0$, depicting the z dependence of both the potential and the ground-state electron density is shown in Fig. 3.

The ''bottom of the band energy'' of the electrode is about $-0.26\,E_h$ and $-0.24\,E_h$ for the R and C systems, respectively. Combined with the Fermi energy orbitals, we obtain a Fermi kinetic energy of $\langle\psi_{\mathrm{HOMO}}|(-\hbar^2/2\mu_e)\nabla^2|\psi_{\mathrm{HOMO}}\rangle=5.4$ eV for both systems.[64] The shape of the potential surface at the interface between the lead and the molecule differs in the two systems. In Fig. 1 it is seen that the Kohn–Sham potential of system C allows a barrierless passage of electrons (through the openings denoted by arrows) from the jellium electrodes into the carbon channel. In the R-system, there is a slight barrier of 1 eV or less depending on the angle of entrance (see Fig. 1); this barrier is, however, much less in energy than the potential in the electrodes.

To explore the effect of the Kohn–Sham potential on conductance, we first compute the dc conductance within the simple Landauer (the frozen SCF) approach developed in Sec. II E. This calculation takes no account of the screening of the driving bias potential by the electrons and is thus not appropriate for quantitative conductance calculations. Nonetheless, it sheds light on the role the KS potential has in determining the conductance. Within this approximation, we find that the C-system has conductance of $0.4\,g_0$, whereas the R-system's conductance is a factor of 20 lower, $0.02\,g_0$.

This rather large difference cannot be explained by the existence of small barriers at the interface of the R-system since the kinetic energy of the electrons coming from the jellium is in excess of 5 eV. The 20-fold enhancement in conductivity of the C- as compared to the R-system is probably due to the more efficient energy transfer between the lateral and vertical electron modes in the former case. Quantum mechanically, to efficiently cross the channel, the lateral (x/y) direction of the electronic wave function must have a wavelength comparable to or smaller than the aperture diameter $D=4.5a_0$). For this, the electron must convert some of its energy into kinetic energy in the lateral direction. This means that a large increase in the *perpendicular* kinetic energy must be achieved in order to cross the channel from one

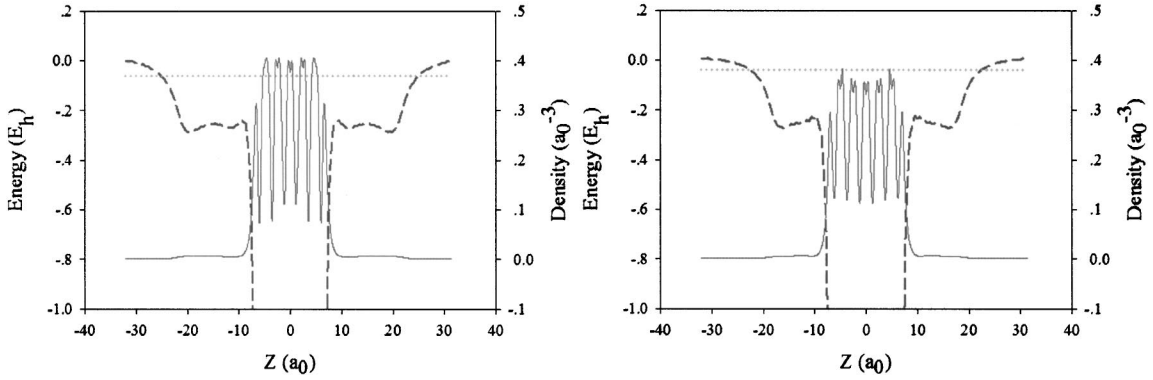

FIG. 3. The electron density (solid lines) and Kohn–Sham potential (broken lines) in the R-system (left) and C-system (right). The energy of the Fermi level in each system is depicted as a dotted line.

jellium slab to the other. Thus, conductance in the z direction is possible only if efficient acceleration in the $x-y$ directions is present. If this kinetic energy conversion is inefficient, the length of the channel will be important: conductance will drop exponentially with length. This is despite the fact that the molecular channel has no *apparent* high barriers. By inspection of the Kohn–Sham potential energy surfaces (KSPESs) in Fig. 1, it is visibly clear that the KSPES in the C-system has gradients pointing in the perpendicular directions at the entrance of the channel. This allows the electrons of the C-system to easily accelerate in the perpendicular directions and thus facilitates conduction. In the R-system, the KSPES restricts the electrons to a small angle, where there are very little perpendicular forces with which to accelerate the electrons in the $x-y$ directions. In addition, from inspection, it is evident that the length of the constriction in the R-system is about 15 a_0—twice as large as in the C-system.

These considerations dominate the conductance. Even when other important effects, such as screening and dynamic excitations are taken into account by the more rigorous method used in the next section, the geometric effect described here still dictates that the R-system conducts much less well than the C-system.

B. TDLDA dc conductance of the C_6 systems

In order to study the dc conductance, we start with a system in its ground state and suddenly turn on a small electric field

$$v_{\mathrm{ext}}(\mathbf{r},t)=v_{\mathrm{nuc}}(\mathbf{r})+f(t)eEz, \tag{2.20}$$

where

$$f(t)=\begin{cases} 1 & t>T \\ \sin^2(\pi t/2T) & T>t>0 \\ 0 & 0>t\,, \end{cases} \tag{2.21}$$

and the parameters are given in Table I. This almost sudden change of conditions causes a small time-dependent current density $\mathbf{j}(\mathbf{r},t)$ to form, the dc component of which is absorbed by the imaginary potential. The dc current is the time average of the current density

$$\mathbf{j}_{DC}(\mathbf{r})=\lim_{t\to\infty}\frac{1}{t}\int_0^t \mathbf{j}(\mathbf{r},\tau)d\tau. \tag{2.22}$$

The y-averaged current density $\langle \mathbf{j}_{dc}(x,z)\rangle_y = 1/L_y \int_0^{L_y}\mathbf{j}_{dc}(x,y,z,t)dy$, is shown in Fig. 4, superimposed on an $x-z$ cut of the Kohn–Sham potential energy surface. (Note: the largest arrow length in each figure is constant and hence arrow lengths in different figures should not be compared.)

The dc conductance that is obtained from the TDLDA calculations is simply the inverse $\omega=0$ impedance, calculated from Eq. (2.9). In Table II we report the TDLDA result and compare it with the simple Landauer-based approximation of Sec. II E. The observed discrepancy is expected, as the latter calculation completely neglects the effect of the bias potential. Within that approximation applying a bias potential is problematic because it is not possible to determine how well the dynamic response of the electrons will screen it. This response is explicitly taken into account in the TDLDA treatment.

The computed conductance for the C-system is in excellent agreement with the calculation of Lang and co-workers,[43] who studied this system within a nonequilibrium Green's function approach. The agreement is expected since both methods take screening into proper account.

Close inspection reveals that the dc current density is generally uniform in the channel at short times, decreasing only near the steep walls. In the C-system, the dc current enters the channel from the right, rapidly making a left turn after entrance. This shows that the C-system has the desired $z-y$ and $z-x$ coupling discussed in the previous section, which facilitates the conduction. This effect is missing in the R-system. The symmetry breaking is a result of the small symmetry breaking in the potential which results from the system being small.

C. Characteristics of the ac current

Subtracting the dc term from the total current density $\mathbf{j}$ leaves an oscillating current, several snapshots of which are seen in Fig. 5 for the R-system. One prominent feature of the current density fluctuations is the uniform flow in the mo-

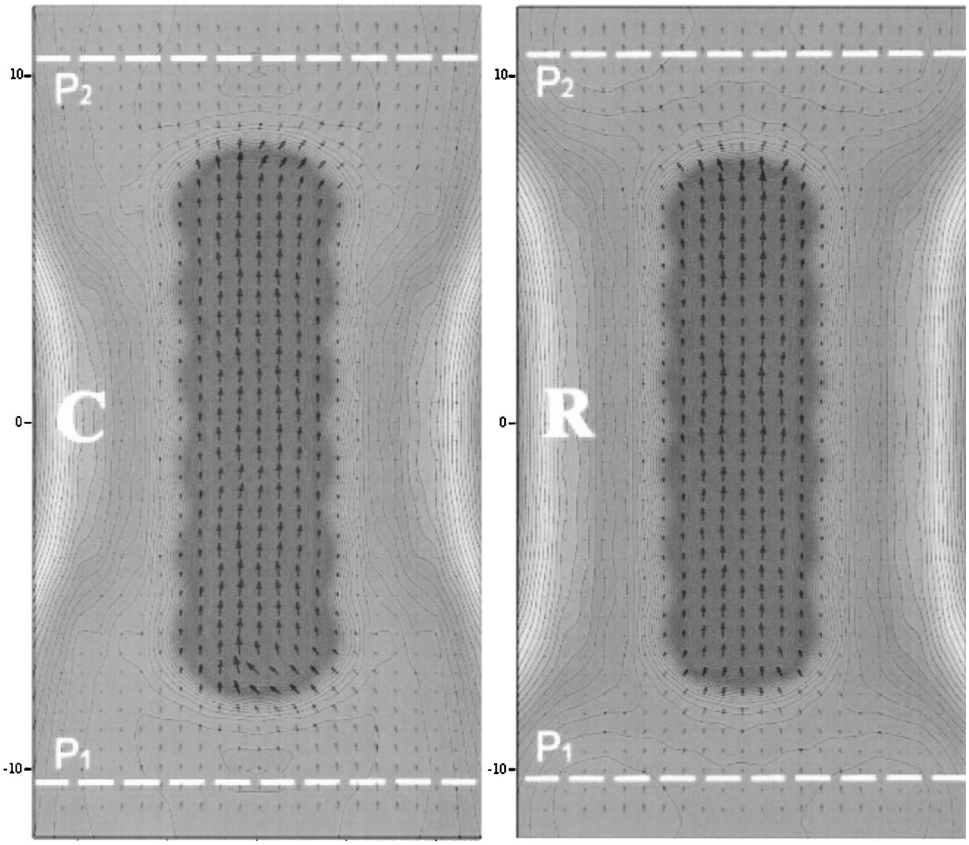

FIG. 4. The dc current density for a ramp pulse, superimposed on the Hartree potential. Arrow lengths are normalized separately in each plate.

lecular channel at short times. Only in one of the frames the flow exhibits significant nonuniformity. This is an indication that the fluctuations of the current are caused by collective oscillations.

The solid curve of Fig. 6 shows the calculated absorption cross section of an isolated jellium slab. The spectrum exhibits strong plasma oscillations at 3.75, 5.1, and 5.6 eV. The redshifts from the surface plasmon frequency of gold (at 6.4 eV) are due to the thin slabs used. In general, we find that the thinner the slabs the lower the plasmon frequency.[65] Also shown in Fig. 6 is the electronic absorption spectrum of the C_6 molecule, which exhibits a strong absorption peak at 6 eV. The Fourier spectrum of the time-dependent current, presented in Fig. 7, can be readily interpreted in terms of the absorption peaks of the device components of Fig. 6, although the strong coupling of the molecule to the electrodes gives rise to substantial broadening. This is especially evident for the C-system. The conclusion of this analysis is that, although the ac current is not limited to ''eigenenergies,'' it does have some peaks associated with the excitation energies of the individual elements of the system.

TABLE II. The dc conductance of the R- and C-systems in the simple Landauer and the TDLDA calculation.

	Landauer	TDLDA
$g(C)/g_0$	0.38	1.30
$g(R)/g_0$	0.02	0.12
$g(C)/g(R)$	19.00	10.80

D. The impedance of the molecular wire

The impedance of the J–C_6–J system is described by polar plots (Figs. 8 and 9). At low frequencies, the real (absorptive) part of the impedance is an even function of the frequency:[19] $Z_r = R + \gamma_1 \omega^2 + O(\omega^4)$, while the imaginary (reactive) part is an odd function of ω: $Z_i = \gamma_2 \omega + O(\omega^3)$. This leads to an analysis of the observed behavior in terms of RLC circuitry,[19] where a resistor R, capacitor C, and inductor L have impedances of R, $i\omega L$, and $-i/\omega C$. The real part of Z is indeed positive for all frequencies. In the R-system, the lower frequency part of spectrum (up to about 2 eV) is strictly negative, indicating ''resistor–capacitor'' type of behavior. At the high-frequency end of the spectrum (above 4 eV) the imaginary part is positive and a resistor–inductor character sets in.

For any but very low frequencies the Taylor-type expansion is not valid. Yet, we find the impedance of the R-system still has a simple structure. It can be described as a combination of circular arcs in the complex plane

$$Z(\omega) = Z_a - re^{-i(\omega-\omega_0)\tau}, \tag{2.23}$$

parametrized by the frequency ω. The center of the arc is at Z_a and its radius is r. τ is the rate at which the arc is transversed and ω_0 controls its initial phase. Each arc is defined for a certain frequency range. For example, we determined using least-square fit the parameters for three arcs of the R-system, as given in Table III.

The C-system too has the impedance composed of arcs. Yet, at low frequencies it behaves quite differently from that

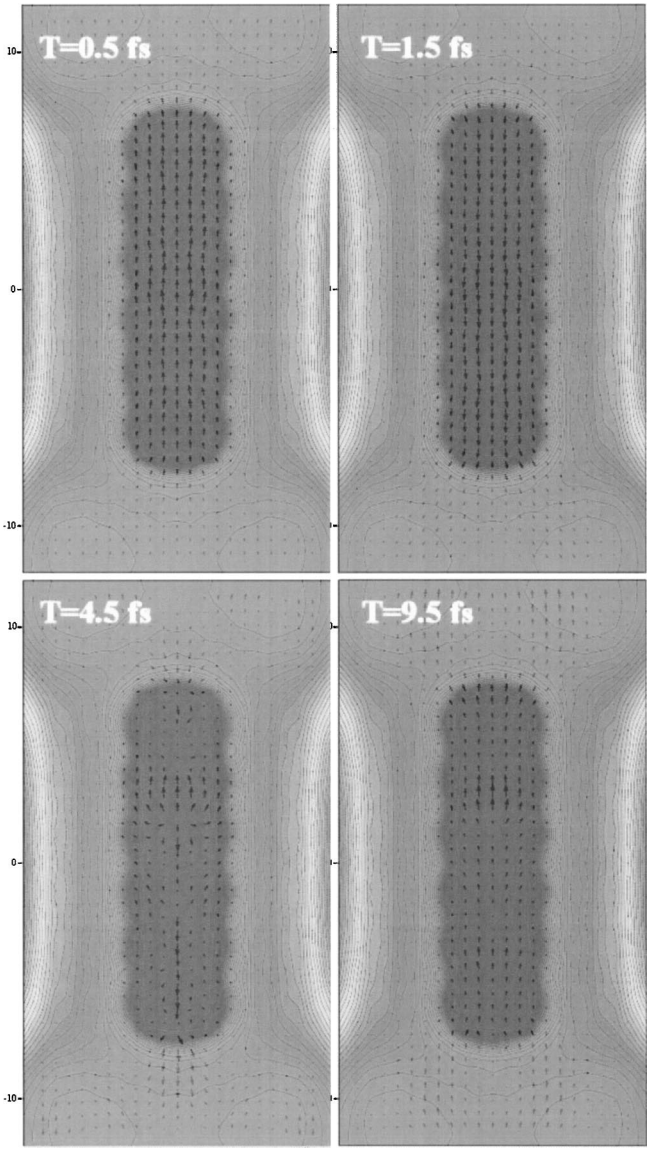

FIG. 5. Some snapshots of the current density for the R-system. The most notable feature is the uniformity of the direction of flow, observed in the short-time snapshots. In each snapshot, the length of the longest arrow is a constant.

of the R-system. In fact, the imaginary part of the impedance is essentially always positive; thus, this system has a resistor–inductor character.

IV. SUMMARY AND DISCUSSION

In this paper we presented a novel approach to calculating the electronic transport properties of molecular junctions. We developed a method that in principle takes into account important effects at zero bias, namely the accurate static density and dynamic response of the electronic system. In addition, we presented a novel Monte Carlo method for an efficient application to Landauer-type conductance calculations. We have also seen that useful insight into the conductance mechanism of molecular devices can be gained by examination of the underlying Kohn–Sham potential. The latter require a relatively minor computational effort.

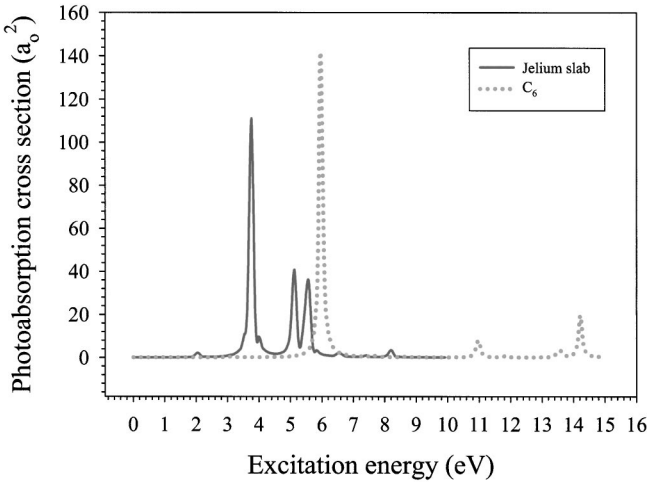

FIG. 6. The calculated photoabsorption cross section of a single jellium slab and an isolated C_6 molecule (both assumed in the singlet ground state). In both cases, the electric polarization is assumed along the long axis. In calculating the cross sections, a phenomenological decay rate of 0.1 fs^{-1} was assumed.

We examined two systems. The R- and C-systems both show good barrierless coupling to the leads in their ground state, calculated by LDA. Yet, the conductance in these systems was very different. In the C-system the conductance was a factor of 20 larger than the R-system. This was explained as a result of a geometric effect: electrons need to be able to accelerate in the vertical direction, in order to mount the conducting channel. The KSPES of the C-system facilitates such acceleration while the R-system does not.

An additional striking difference between the two systems is their ac impedance, being of completely different qualitative nature. The R-system exhibits capacitor-like behavior at low frequencies, similar to a capacitor and resistor connected in parallel. At high frequency the R-system is more like a resistor–inductor. The C-system exhibits resistor–inductor characteristics throughout. The impedance

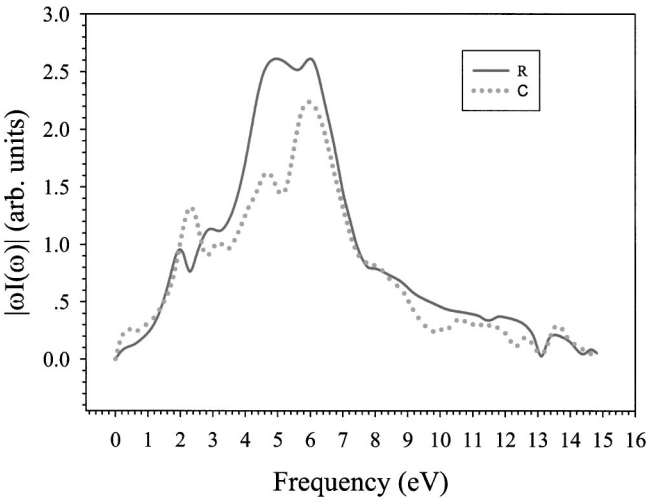

FIG. 7. The spectrum of the current in the R- and C-systems. The spectrum is very wide, but shows peaks at the absorption lines of its separate constituents (compare with Fig. 6).

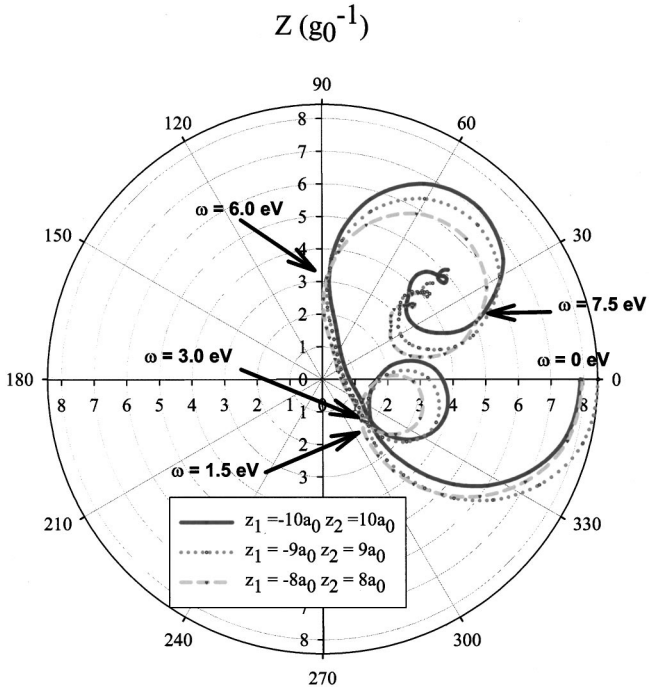

FIG. 8. Polar plot of the complex impedance of the R-system for several potential-probe locations, as indicated. Each trajectory starts on the real axis where the impedance is the dc resistance (zero frequency) and ends at a frequency corresponding to 10 eV.

curve in the complex plane can be described by a series of parametrized arcs. Each arc is highly circular in nature, with a well-defined center and radius.

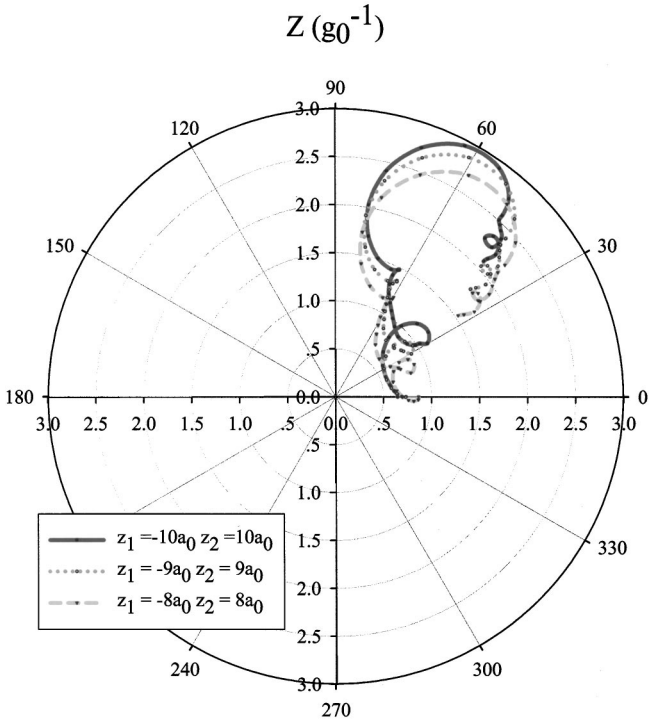

FIG. 9. Polar plot of the complex impedance of the C-system for several contact measurements, as indicated. Each trajectory starts on the real axis where the impedance is the dc resistance (zero frequency) and ends at a frequency corresponding to 10 eV.

TABLE III. Best-fit impedance parameters [Eq. (2.23)] for several frequency ranges.

Freq. range eV/$\hbar$	$Z_a\ g_0^{-1}$	$r\ g_0^{-1}$	ω_0 eV/$\hbar$	$\tau\ \hbar$/eV
$\omega<1.5$	$3.9+0.4i$	3.6	1.9	1.5
$1.5<\omega<3.0$	$2.4-0.8i$	1.6	0.3	4.5
$6.0<\omega<7.5$	$2.7+2.9i$	2.8	1.1	2.5

While the present calculation has made a step towards understanding the intricacies of conductance in molecules, there are still open questions for future research. One question left unanswered is the degree of appropriateness of LDA for studying molecular conductance. This is studied by performing high-level calculations and comparing to high-quality experimental data. There are causes for concern: the theory may not be capable of correctly treating conductance when it is controlled by a Coulomb blockade effect. Experiments indicate that Coulomb blockade effects may be of cardinal importance.[11] Nuclear motion and possibly other ''inelastic'' effects may also have an effect on the conductance[66] and we have neglected it in this study. We have not used optimized structures for this study, although we did make separate optimizing calculation and found that the molecule slightly dimerizes (a Peierls distortion sets in). The effect of this will be studied in a future publication.

In spite of these deficiencies, it is clear that TDDFT provides an efficient and rigorous framework for calculating both dc and ac conductance properties. Although, to our knowledge, the ac properties of molecular junctions have not been studied experimentally as yet, these properties are expected to become important in the future, as the interaction of light and high-frequency fields with molecular devices is implemented, as well as the interaction of several molecular devices concurrently. It is expected that future applications of TDDFT to molecular-scale conductance would trigger this and other advances of the theory.

ACKNOWLEDGMENTS

We gratefully acknowledge Mark Ratner and Abraham Nitzan for their useful comments on the manuscript. This research was funded by the Israel Science Foundation.

[1] M. Bockrath, D. H. Cobden, P. L. McEuen, N. G. Chopra, A. Zettl, A. Thess, and R. E. Smalley, Science **275**, 1922 (1997).
[2] M. A. Reed, C. Zhou, C. J. Muller, T. P. Burgin, and J. M. Tour, Science **278**, 252 (1997).
[3] C. Kergueris, J. P. Bourgoin, S. Palacin, D. Esteve, C. Urbina, M. Magoga, and C. Joachim, Phys. Rev. B **59**, 12505 (1999).
[4] S. Creager, C. J. Yu, C. Bamdad *et al.*, J. Am. Chem. Soc. **121**, 1059 (1999).
[5] K. Slowinski, H. K. Y. Fong, and M. Majda, J. Am. Chem. Soc. **121**, 7257 (1999).
[6] X. D. Cui, A. Primak, X. Zarate, J. Tomfohr, O. F. Sankey, A. L. Moore, T. A. Moore, D. Gust, G. Harris, and S. M. Lindsay, Science **294**, 571 (2001).
[7] M. L. Chabinyc, X. X. Chen, R. E. Holmlin, H. Jacobs, H. Skulason, C. D. Frisbie, V. Mujica, M. A. Ratner, M. A. Rampi, and G. M. Whitesides, J. Am. Chem. Soc. **124**, 11730 (2002).
[8] J. G. Kushmerick, D. B. Holt, J. C. Yang, J. Naciri, M. H. Moore, and R. Shashidhar, Phys. Rev. Lett. **89**, 086802 (2002).

[9] D. Porath, A. Bezryadin, S. de Vries, and C. Dekker, Nature (London) **403**, 635 (2000).
[10] M. S. Fuhrer, J. Nygard, L. Shih *et al.*, Science **288**, 494 (2000).
[11] J. Park, A. N. Pasupathy, J. I. Goldsmith *et al.*, Nature (London) **417**, 722 (2002).
[12] H. B. Weber, J. Reichert, F. Weigend, R. Ochs, D. Beckmann, M. Mayor, R. Ahlrichs, and H. von Lohneysen, Chem. Phys. **281**, 113 (2002).
[13] N. B. Zhitenev, H. Meng, and Z. Bao, Phys. Rev. Lett. **88**, 226801 (2002).
[14] A. Nitzan and M. A. Ratner, Science **300**, 1384 (2003).
[15] J. Jortner and M. Ratner, *Molecular Electronics* (Blackwell Science, New York, 1997).
[16] These relations hold when there are no phase coherent effects between components. This can happen, for example, when the distance between the components is much larger than the electronic phase relaxation length.
[17] A. P. Jauho, N. S. Wingreen, and Y. Meir, Phys. Rev. B **50**, 5528 (1994).
[18] L. Chen and C. Ting, Phys. Rev. Lett. **64**, 3159 (1990).
[19] G. Cuniberti, M. Sassetti, and B. Kramer, Phys. Rev. B **57**, 1515 (1998).
[20] S. Datta and M. P. Anantram, Phys. Rev. B **45**, 13761 (1992).
[21] A. Tikhonov, R. D. Coalson, and Y. Dahnovsky, J. Chem. Phys. **117**, 567 (2002).
[22] A. Tikhonov, R. D. Coalson, and Y. Dahnovsky, J. Chem. Phys. **116**, 10909 (2002).
[23] J. Lehmann, S. Kohler, P. Hanggi, and A. Nitzan, Phys. Rev. Lett. **88**, 228305 (2002).
[24] J. Lehmann, S. Kohler, P. Hanggi, and A. Nitzan, J. Chem. Phys. **118**, 3283 (2003).
[25] R. Landauer, IBM J. Res. Dev. **1**, 223 (1957).
[26] S. Datta, *Electronic Transport in Mesoscopic Systems* (Cambridge University Press, Cambridge, 1995).
[27] Y. Imry and R. Landauer, Rev. Mod. Phys. **71**, S306 (1999).
[28] R. Baer and D. Neuhauser, J. Am. Chem. Soc. **124**, 4200 (2002).
[29] D. Walter, D. Neuhauser, and R. Baer, Chem. Phys. (to be published).
[30] C. Liu, D. Walter, D. Neuhauser, and R. Baer, J. Am. Chem. Soc. **125**, 13936 (2003).
[31] R. Baer and D. Neuhauser, Chem. Phys. **281**, 353 (2002).
[32] C. Joachim and J. F. Vinuesa, Europhys. Lett. **33**, 635 (1996).
[33] V. Mujica, A. Nitzan, Y. Mao, W. Davis, M. Kemp, A. Roitberg, and M. A. Ratner, Adv. Chem. Phys. **107**, 403 (1999).
[34] M. Buttiker and H. Thomas, *Quantum-Effect Physics, Electronics and Applications* (Institute of Physics and Physical Society, Bristol, 1992).
[35] M. Buttiker, A. Pretre, and H. Thomas, Phys. Rev. Lett. **70**, 4114 (1993).
[36] K. Hirose and M. Tsukada, Phys. Rev. B **51**, 5278 (1995).
[37] V. Mujica, A. E. Roitberg, and M. Ratner, J. Chem. Phys. **112**, 6834 (2000).
[38] S. Pleutin, H. Grabert, G. L. Ingold, and A. Nitzan, J. Chem. Phys. **118**, 3756 (2003).
[39] P. Damle, A. W. Ghosh, and S. Datta, Chem. Phys. **281**, 171 (2002).
[40] M. Di Ventra, S. T. Pantelides, and N. D. Lang, Phys. Rev. Lett. **84**, 979 (2000).
[41] Y. Q. Xue, S. Datta, and M. A. Ratner, Chem. Phys. **281**, 151 (2002).
[42] J. Taylor, H. Guo, and J. Wang, Phys. Rev. B **63**, 245407 (2001).
[43] N. D. Lang and P. Avouris, Phys. Rev. Lett. **81**, 3515 (1998).
[44] N. D. Lang and P. Avouris, Phys. Rev. Lett. **84**, 358 (2000).
[45] R. Baer and D. Neuhauser, Int. J. Quantum Chem. **91**, 524 (2003).
[46] We have checked that the dc impedance is not affected by the choice of the point where the current is computed. The ac impedance may be sensitive to such a choice. This is not an artifact: an experiment will also have to define the exact choice of points of measurement of the current.
[47] M. Caspary, L. Berman, and U. Peskin, Chem. Phys. Lett. **369**, 232 (2003).
[48] Y. Oreg and A. M. Finkelstein, Phys. Rev. B **54**, 14265 (1996).
[49] E. Runge and E. K. U. Gross, Phys. Rev. Lett. **52**, 997 (1984).
[50] G. Vignale and W. Kohn, Phys. Rev. Lett. **77**, 2037 (1996).
[51] P. L. de Boeij, F. Kootstra, J. A. Berger, R. van Leeuwen, and J. G. Snijders, J. Chem. Phys. **115**, 1995 (2001).
[52] M. K. Harbola and A. Banerjee, Phys. Rev. A **60**, 5101 (1999).
[53] J. P. Perdew and Y. Wang, Phys. Rev. B **45**, 13244 (1992).
[54] N. Troullier and J. L. Martins, Phys. Rev. B **43**, 1993 (1991).
[55] M. Fuchs and M. Scheffler, Comput. Phys. Commun. **119**, 67 (1999).
[56] D. Neuhauser and M. Baer, J. Chem. Phys. **90**, 4351 (1989).
[57] R. Baer and D. Neuhauser, Chem. Phys. Lett. **374**, 459 (2003).
[58] A. Nitzan, Annu. Rev. Phys. Chem. **52**, 681 (2001).
[59] U. V. Riss and H. D. Meyer, J. Chem. Phys. **105**, 1409 (1996).
[60] T. Seideman and W. H. Miller, J. Chem. Phys. **97**, 2499 (1992).
[61] A detailed account of the method will be published separately.
[62] T. Iitaka, S. Nomura, H. Hirayama, X. W. Zhao, Y. Aoyagi, and T. Sugano, Phys. Rev. E **56**, 1222 (1997).
[63] R. Baer, M. Head-Gordon, and D. Neuhauser, J. Chem. Phys. **109**, 6219 (1998).
[64] We note that for these small slabs the energy of the HOMO is not a good estimate of the ionization energy. In this system, the HOMO energy is about -1.5 eV, the EN-1-EN energy is -4.2 eV.
[65] R. Baer, S. Weiss, and D. Neuhauser, Nano. Lett. (to be published).
[66] D. Segal and A. Nitzan, Chem. Phys. **281**, 235 (2002).